The 2018 Structures Congress (Structures18)
Songdo Convensia, Incheon, Korea, August 27 - 31, 2018

Shape change of spine biotensegrity model

Chai Lian Oh[1)], Kok Keong Choong[2)], Toku Nishimura[3)],
Jae-Yeol Kim[4)] and Sang Hyun Jeon[5)]

[1)] *Faculty of Civil Engineering, University Teknologi MARA 40450 Shah Alam, Selangor Darul Ehsan, Malaysia*
[2)] *School of Civil Engineering, University Sains Malaysia, Malaysia*
[3)] *Department of Architectural Engineering, Institute of Disaster and Environmental Science, Kanazawa Institute of Technology, Ishikawa, Japan*
[4), 5)] *Department of Architectural Engineering, Hyupsung University, Hwasung-shi, Gyeongi-do, Republic of Korea*
[1)]*chailian_o80@yahoo.com*

ABSTRACT

Biotensegrity as a model emulated from the forms and functions of hierarchical biological system possesses great potential in shape change ability. Despite extensive investigations on deployability of tensegrity structures, there is limited study on the shape change of biotensegrity. This paper presents a computational investigation on the shape change of spine biotensegrity model. The paper describes the computational method in two parts: (1) the incremental equilibrium equations, and (2) optimization forced elongation of the cables for shape change purpose. The proposed method is applied to a self-equilibrated four-stage class 1 spine biotensegrity model. In this paper, ability of the spine biotensegrity model to undergo shape change in uni-directional mode particularly in *x*- direction were investigated.

Keywords: Shape change, biotensegrity, tensegrity, optimization, simulation

1. INTRODUTION

Biotensegrity was initiated by Levin [1] and Ingber, et al. [2] since 1980's. The principle applies human made tensegrity structures in explaining the architectures and mechanics of biological systems. The mechanism of contraction and expansion in organisms has been described via biotensegrity system consisting compressive and tension components. Biotensegrity as one of the biomechanical models is capable in simulating the processes of sensing, signalling and providing feedback in organism. Chen, et al. [3] even claim that tensegrity model as the most potential mechanical cellular model for the study of mechanisms of living cells.

Inspiration from tensegrity for robotic application attracts many researchers for the past decade. For instance, Paul, et al. [4] investigated the forward locomotion of tensegrity prisms (Figure 1a) whereas Shibata, et al. [5] examined the crawling ability of a six-strut tensegrity robot experimentally. Juan and Tur [6] proposed a method considering a quasi-static case to detect and further avoid collisions within internal structure elements and with surrounding obstacles. This investigation suggested transformable modular robot that was able to avoid unnecessary obstacles as well as to squeeze in a narrow space.

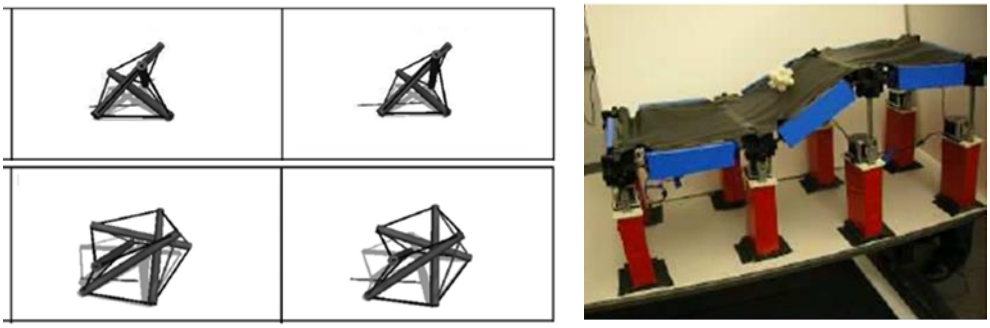

(a) (b)

Figure 1: Robots using (a) tensegrity prism [4] (b) biotensegrity principle, Morpho [7]

However, limited study has been conducted on tensegrity based robots that mimic biological architecture and mechanical system. A modular robot namely Morpho (Figure 1b) mimicking the expansion and contraction mechanism in cells was constructed by Yu, et al. [7]. This robot was recommended as a tool to explore narrow space, expandable structural columns, and prosthetic device for human motion. To address the gap, this paper presents a computational investigation on the shape change of biotensegrity model mimicking human spine.

The remainder of the paper is organized as follows. Section 2 presents the details of the proposed shape change strategies for spine biotensegrity models. Section 3 shows the simulation results for shape change of spine biotensegrity models in uni-directional. Finally, Section 4 shows the conclusions of the paper.

2. SHAPE CHANGE OF SPINE BIOTENSEGRITY MODELS

2.1 Generation of spine biotensegrity models

Geometrical input data of spine biotensegrity models were gathered from anatomical dimension of human spine by Busscher, et al. [8]. The human spine specimens were collected from six male cadavers with age and body height at death ranging from 55-84 year-old and 175-192 cm respectively (mean of 72 year-old and 182 cm, respectively).

Figure 2 shows a typical vertebra in superior and lateral view. A total of twenty two vertebrae from region cervical (vertebrae C3-C7), thoracic (vertebrae T1-T12) and lumbar (vertebrae L1-L5) were considered in this study (see Figure 3a).

Vertebral end-plate width (EPW) of each vertebra (also taken as the average of upper (UEPW) and lower vertebral end-plate width (LEPW)) represents the width of the spine biotensegrity models. Accumulation of the vertebral central body height (VBHC) and intervertebral disc height (IDH) represents the height of the model whereas accumulation of IDH only represents the saddle height in the model.

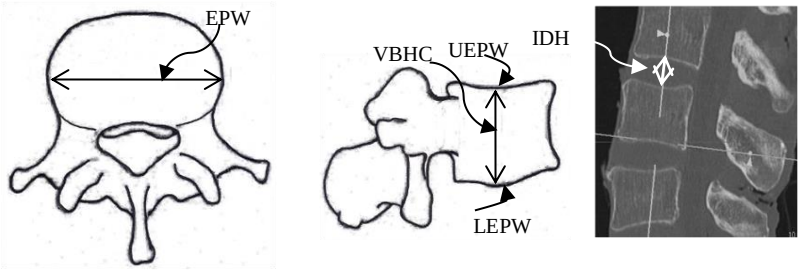

(a) Superior (b) Lateral

Figure 2: Typical vertebra parameters

Generally, human spine (Figure 3a) has a natural curvature in sagittal view with: (i) lordosis (concave curve) at cervical and lumbar region and (ii) kyphosis (convex curve) at thoracic and sacral regions. According to Busscher, et al. [8], cervical lordosis of 20.1^{o}, thoracic kyphosis of 34.5^{o} and lumbar lordosis of 29.2^{o} were measured as the angle between the upper end-plate of C3 and the lower end-plate of C7, between the upper end-plate of T1 and the lower end-plate of T12 and between the upper end-plate of L1 and the lower end-plate of L5, respectively. These angles are reasonably accepted and supported by others [9, 10].

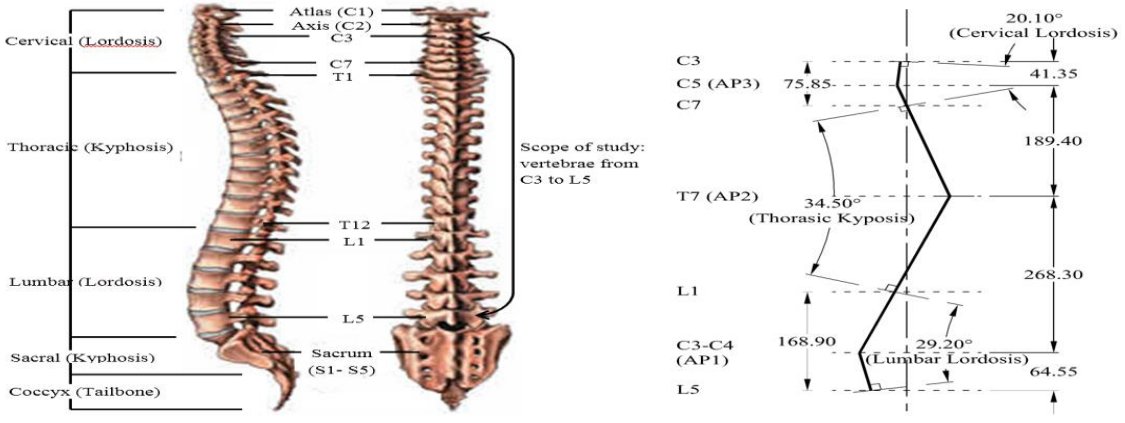

(a) (b)

Figure 3 (a) Human spine anatomy lateral (left) and posterior (right) view [11], (b) Construction of curvature line mimicking human spine

The spine biotensegrity models incorporated the curvature of human spine by adopting the three apexes for cervical lordosis, thorasic kyphosis and lumbar lordosis. The positions of these three apexes are important in determining the placement of individual cell in the models. Figure 3b shows the established natural sagittal line for spine biotensegrity model. The decision on the locations of these apexes was based on several literatures [12-14].

Moreover, the biotensegrity models motivated from the neutral posture of human spine should satisfy the rule of C7 plumb line. In this study, apex of the curvature is defined as the farthest point of a vertebra from C7 plump line which is established by drawing a vertical line extending from center of C7 vertebral body to posterior corner (i.e at the back) of sacrum S1 [15]. The normal weight of human body generally acts through the C7 plumb line. One of the most common methods namely Cobb method has been adopted in establishing the curvature of the spine biotensegrity models. A review on this method is given by Vrtovec, et al. [16]. Form-finding of the spine biotensegrity models has been presented by the authors [17].

2.2 Shape change algorithm

2.2.1 Incremental equilibrium equations

A spine biotensegrity model consists of m elements, n nodes, n_c constrained and n_u ($3n$ - n_c) unconstrained degree of freedoms. Axial forces of the elements in spine biotensegrity model can be determined from the following equation:

$$\boldsymbol{F} = \boldsymbol{B}\boldsymbol{n} \qquad \text{Eq. (1)}$$

where $\boldsymbol{B}$ is a $n_u \times m$ matrix consisting of directional cosines of all elements with respect to x, y, z axes, $\boldsymbol{F}$ is a vector of nodal forces of all nodes with size n_u and $\boldsymbol{n}$ is a vector of axial forces for all elements with size m.

The initial axial forces of the models (i.e. prestress) was obtained via form-finding process without the application of external forces to the system (i.e. $\boldsymbol{F}$ = **0)** [17]. The spine biotensegrity models searched from form-finding process were further fixed supported at the three nodes located at base and subjected to self-weight. The self-weight was applied as concentrated loads to all nodes within the spine biotensegrity models.

At each incremental step during shape change analysis (i.e. step t), the vector of current nodal coordinates of the biotensegrity model could be expressed as

$$^{t}\boldsymbol{x} = {}^{t-1}\boldsymbol{x} + {}^{t}\dot{\boldsymbol{x}} \qquad \text{Eq. (2)}$$

where the vector of incremental nodal coordinates, ${}^{t}\dot{\boldsymbol{x}}$ is derived from the equilibrium equation:

$$^{t}\dot{\boldsymbol{x}} = \boldsymbol{K}^{-1}\boldsymbol{F} \qquad \text{Eq. (3)}$$

The vector of nodal coordinates of the monitored nodes with size n_u is denoted as $\boldsymbol{x}$. Left superscripts t-1 and t denotes the previous step and current step, respectively. $\boldsymbol{K}$ is the stiffness matrix of size $n_u \times n_u$ consisting of the axial forces and the directional cosines.
Since the stiffness matrix of tensegrity structure with the introduction of appropriate self-equilibrium stresses is positive-definite, the inverse of the stiffness matrix exists.
Axial force of an element of biotensegrity model at step t could be defined as

$$^{t}\boldsymbol{n} = {}^{t-1}\boldsymbol{n} + {}^{t}\dot{\boldsymbol{n}} \qquad \text{Eq. (4)}$$

Assuming the element is linear elastic with axial stiffness EA, with the known length, ^{t-1}l and elastic elongation, ^{t-1}u, the incremental axial force is determined as

$$^{t}\dot{n} = EA\left(\frac{^{t}\dot{u}}{^{t-1}l} - \frac{^{t-1}u\,{}^{t}\dot{l}}{^{t-1}l^{2}}\right) \qquad \text{Eq. (5)}$$

where E and A denote the Young modulus and cross sectional area of an element in biotensegrity model, respectively.

The incremental elastic elongation, $^{t}\dot{u}$ without the consideration of force elongation (i.e. $^{t}\dot{l}$=0) could be determined from the equation:

$$^{t}\dot{\boldsymbol{u}} = \boldsymbol{B}^{T}\,{}^{t}\dot{\boldsymbol{x}} \qquad \text{Eq. (6)}$$

2.2.2 Optimization

The vector for the incremental nodal coordinates, $^{t}\dot{\boldsymbol{x}}$ and the incremental axial forces, $^{t}\dot{\boldsymbol{n}}$ during shape change could be expressed in terms of force elongation as the following equations:

$$^{t}\dot{\boldsymbol{x}} = {}^{t}\boldsymbol{K}^{-1}\,{}^{t}\boldsymbol{B}\,{}^{t}\boldsymbol{C}_{\mathrm{L}}\,{}^{t}\dot{\boldsymbol{l}} \qquad \text{Eq. (7)}$$

and

$$^{t}\dot{\boldsymbol{n}} = {}^{t}\boldsymbol{D}_{2}\,{}^{t}\dot{\boldsymbol{l}}$$
$$^{t}\boldsymbol{D}_{2} = \left({}^{t}\boldsymbol{C}_{1}\,{}^{t}\boldsymbol{B}^{T}\,{}^{t}\boldsymbol{K}^{-1}\,{}^{t}\boldsymbol{B} - \boldsymbol{I}_{m}\right){}^{t}\boldsymbol{C}_{L} \qquad \text{Eq. (8)}$$

where

$$\boldsymbol{C}_{Li} = \frac{E_i A_i}{^{t-1}l_i}\left(1 + \frac{^{t-1}u_i}{^{t-1}l_i}\right);\ \boldsymbol{C}_{1i} = \frac{E_i A_i}{^{t-1}l_i} \qquad \text{Eq. (9)}$$

Objective function aiming to minimize the distance between the monitor nodes and target coordinates was set as

$$\min f(x) = \left| {}^{t}\boldsymbol{x} - \bar{\boldsymbol{x}} \right| \qquad \text{Eq. (10)}$$

where $\bar{\boldsymbol{x}}$ is the prescribed target coordinates, and ${}^{t}\boldsymbol{x}$ is the current coordinates (see Equation (2)), for all the specified monitored nodes at current step during the shape change analysis.

The incremental nodal coordinates for the specified monitored nodes, ${}^{t}\dot{\boldsymbol{x}}$, are extracted from the vector of incremental nodal coordinates of all nodes in tensegrity models, ${}^{t}\dot{\boldsymbol{x}}$, (see Equation (7)) by introducing matrix $\boldsymbol{P}_1$ as follows:

$${}^{t}\dot{\boldsymbol{x}} = \boldsymbol{P}_1 \, {}^{t}\dot{\boldsymbol{x}} \qquad \text{Eq. (11)}$$

Matrix $\boldsymbol{P}_1$ with size of $n_{utg} \times n_u$, contains information about the prescribed target coordinates of the monitored nodes. n_{utg} denotes number of target coordinates.
By substitution of Equation (7), Equation (11) could be rewritten as

$$\begin{aligned} {}^{t}\dot{\boldsymbol{x}} &= \boldsymbol{P}_2 \, {}^{t}\dot{\boldsymbol{l}} \\ \boldsymbol{P}_2 &= \boldsymbol{P}_1 \left({}^{t}\boldsymbol{K}^{-1} \, {}^{t}\boldsymbol{B} \, {}^{t}\boldsymbol{C}_L \right) \end{aligned} \qquad \text{Eq. (12)}$$

where $\boldsymbol{P}_2$ matrix is of size $n_{utg} \times n_m$.

Sequential Quadratic Programming method was used to solve the nonlinear problem in Equation (10) which is approximated quadratically as follows:

$$\begin{aligned} &\min_{x \in R^n} f(\boldsymbol{x}) = \boldsymbol{g}^T \, {}^{t}\dot{\boldsymbol{l}} + \frac{1}{2} \, {}^{t}\dot{\boldsymbol{l}} \boldsymbol{H} \, {}^{t}\dot{\boldsymbol{l}} \\ &\boldsymbol{g} = \boldsymbol{P}_2^{\mathrm{T}} ({}^{t-1}\boldsymbol{x} - \bar{\boldsymbol{x}}) \\ &\boldsymbol{H} = \boldsymbol{P}_2^{\mathrm{T}} \boldsymbol{P}_2 \end{aligned} \qquad \text{Eq. (13)}$$

where forced elongation, ${}^{t}\dot{\boldsymbol{l}}$, is the optimization variable and $\boldsymbol{H}$ is a positive-definite approximation of Hessian matrix of the Lagrangian function. The sequential quadratic programming problem is subjected to inequality constraints from the upper and lower limits of axial forces as well as the limit of the forced elongation. Figure 4 summarizes the shape change algorithm for spine biotensegrity models.

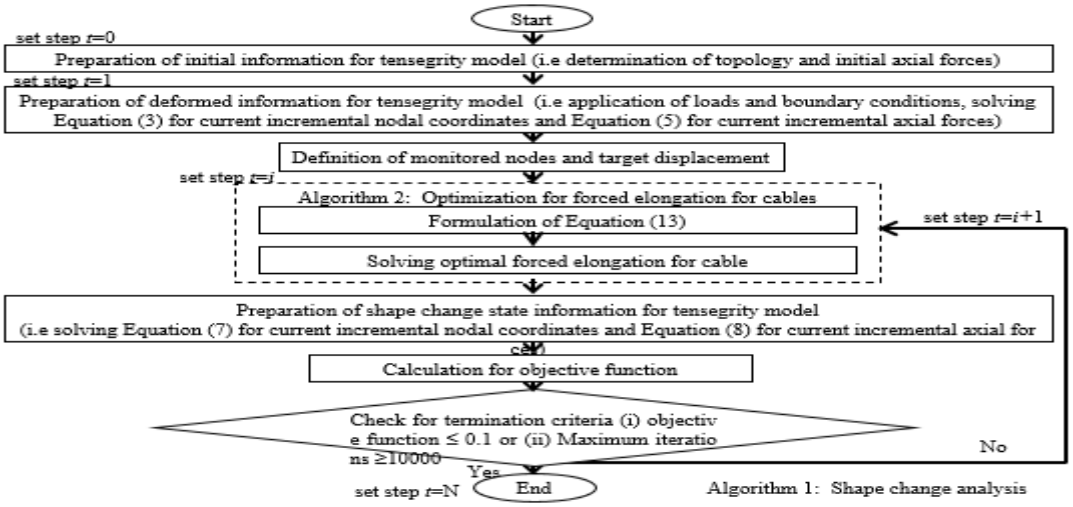

Figure 4: Algorithm for shape change analysis

3. NUMERICAL APPLICATIONS

This section presents the numerical application of the proposed shape change algorithm on three spine biotensegrity models with topology obtained from Oh, et al. [17] (i.e. SB1, SB2 and SB3). In the shape change analysis, three nodes from the peak of the models were selected as the monitored nodes. The advancement of these monitored nodes to the prescribed target coordinates was investigated. This section presents the results from the shape change analysis cases of target displacement in uni-directional mode particularly in positive and negative *x*- direction.

In this study, analysis series Xn and Xp denote the cases with target displacements prescribed in positive and negative *x*- direction, respectively. Specifically, analysis case SB2Xn200 denotes the case where a target displacement of 200 mm in negative *x*-direction was set for each of the monitored nodes of spine biotensegrity model SB2.

3.1 Convergence curves

The convergence curves for SB1, SB2 and SB3 for analysis series Xn and Xp are similar. For this reason, only the results for SB2 are presented in this section. Figure 5 shows plot of the normalized objective function (NOF) versus computational steps for shape change analysis.

From Figure 5, similar trends of NOF are observed for both series of Xn and Xp. NOF plots in these series decrease in a nonlinear trend. Besides, the NOF plot reach a plateau with greater than quarter of the total computational step is clearly seen in the case Xp400 (which happened at NOF lower than 0.05).

The efficiency of the proposed algorithm is rechecked by allowing 2% error (where the value of 2% is based on the recorded successful rate of 98.2% in the total computational step of overall shape change study). It is found that, with this allowance, reduction of up to 40% total computational step in cases of target displacements in uni-directional mode could be achieved.

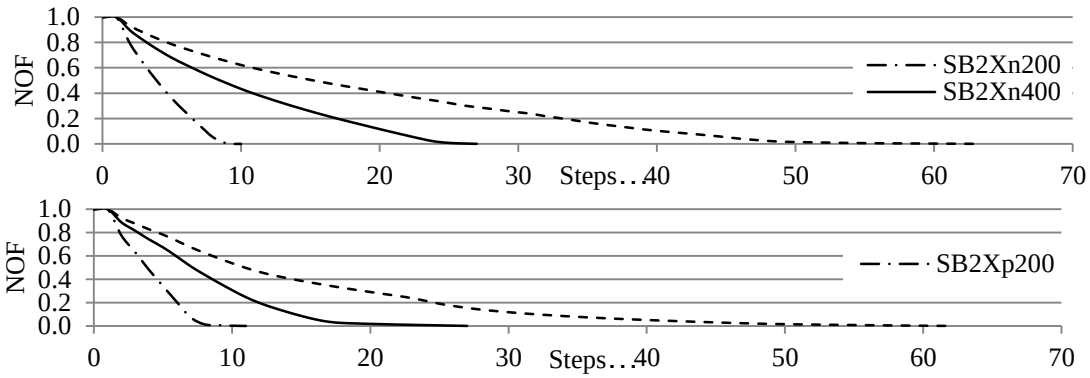

Figure 5: Normalized objective function for cases of uni-directional mode (a) Xn and (b) Xp

3.2 Final configuration of shape change

This section presents the configurations of the spine biotensegrity models at the final computational step of shape change analysis. Figure 6 shows the configuration at step 1 and at final step for shape change analysis series Xn and Xp

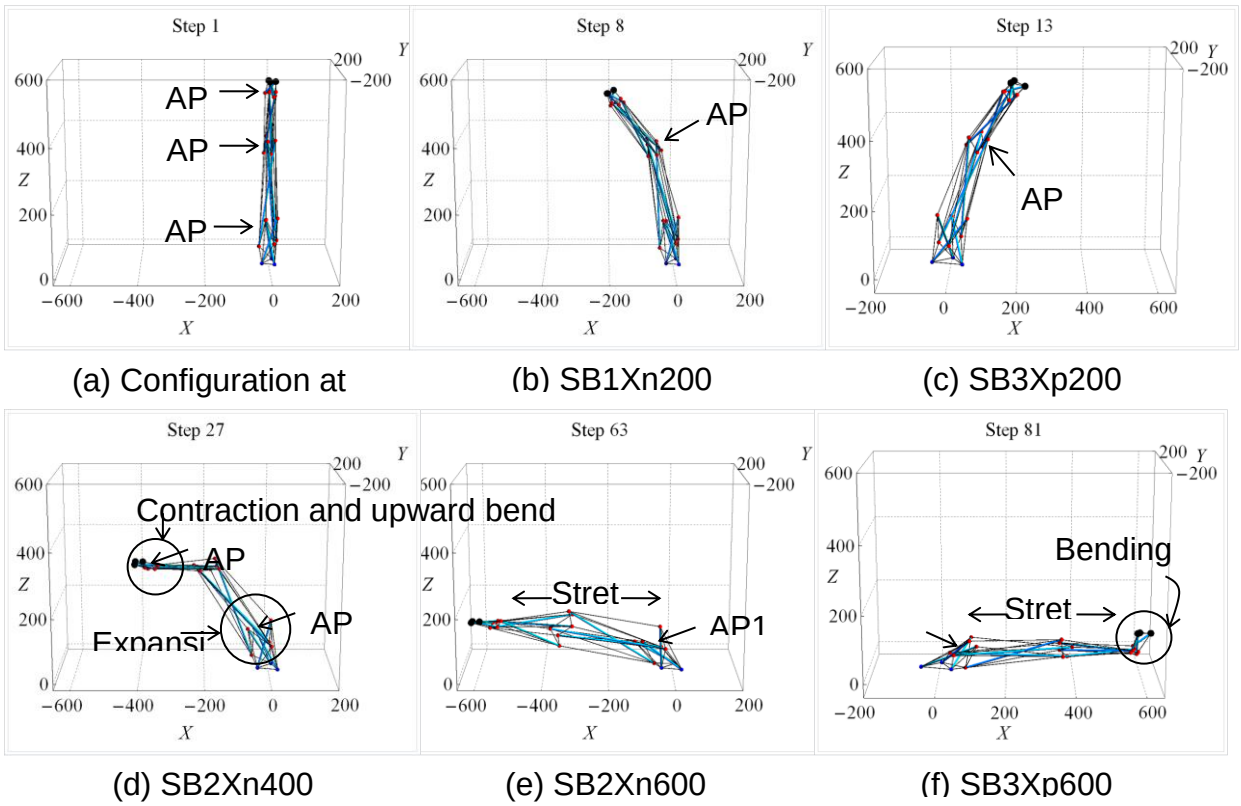

(a) Configuration at (b) SB1Xn200 (c) SB3Xp200

(d) SB2Xn400 (e) SB2Xn600 (f) SB3Xp600

Figure 6: Configuration (a) at step 1 and (b-f) at final step for series Xn and Xp

Generally, the spine biotensegrity models approach to the target coordinates either by bending or combination of axial and bending deformation in series Xn and Xp. There are three apex in the models that play vital role as joints that permit bending (refer Figure 6a for location of AP1, AP2 and AP3). In cases with smaller target displacement magnitude, bending deformation primarily about AP2 is observed in all SBS models (Figure 6b-c). AP1 allows bending only in cases when the target displacement magnitude increases, as shown in Figure 6d-f. Axial deformation accompanied by with bending deformation is observed in analysis cases Xn600 (Figure 6e) and Xp600 (Figure 6f). In most of the cases with larger displacement magnitude, SBS models bend about AP1 and AP3 whereas the segments between the two apex demonstrate stretching (Figure 6d and f). Additionally, the deformations of the models through expansion and contraction are observed. For instance, the large and small clearance between nodes at AP3 and AP1 in analysis case SB2Xn400 (Figure 6d) show the expansion and contraction phenomenon, respectively.

4. CONCLUSIONS

Shape change analysis of biotensegrity models is presented in this paper. Complete convergence of the objective function in shape change analysis of the spine biotensegrity models reveals the effectiveness of the proposed algorithm. The proposed shape change algorithm also ensures non-slackened cables during the analysis. It was found that the computational time for the shape change analysis could be significant reduced with the allowance of inaccurateness in reaching the targets (say 2%).

Simulation results from analysis cases under series Xn and Xp reveal the characteristics of biotensegrity models to undergo bending, axial and combinations of these deformations. Bending deformation was generally observed in all spine biotensegrity models when the target displacement is less than 400mm whereas axial deformation for further target displacement (i.e. 600mm).

The proposed algorithm is suitable for the basic study in the development of deployable structures and biotensegrity robots. The spine biotensegrity model could be adopted as structure with shape change capability for possible use in difficult situations in the construction industry. Future investigation works for shape change of biotensegrity model such as dynamic analysis, control issues, impact from real environmental loadings and operational challenges are recommended.

ACKNOWLEDGEMENTS

This work was supported by the National Research Foundation of Korea (NRF) grant funded by the Korea government (MSIP) (No. 2016R1A2B4014562).

REFERENCES

Levin, S. M. (1982) "Continuous tension, discontinuous compression: a model for biomechanical support of the body," *Bulletin of Structural Integration,* vol. 8.

Ingber, D. E. Madri, J. A. and Jamieson, J. D. (1981) "Role of basal lamina in neoplastic disorganization of tissue architecture," *Proceedings of the National Academy of Sciences,* vol. 78, 3901-3905.

Chen, T.-J. Wu, C.-C. and Su, C.-C. (2012) "Mechanical models of the cellular cytoskeletal network for the analysis of intracellular mechanical properties and force distributions: A review," *Medical Engineering and Physics,* vol. 34, 1375-1386.

Paul, C. Valero-Cuevas, F. J. and Lipson, H. (2006) "Design and control of tensegrity robots for locomotion," *IEEE Transactions on Robotics,* vol. 22, 944-957.

Shibata, M. Saijyo, F. and Hirai, S. (2009) "Crawling by body deformation of tensegrity structure robots," in *Robotics and Automation, 2009. ICRA'09. IEEE International Conference on*, 4375-4380.

Juan S. H. and Tur, J. M. M. (2008) "A method to generate stable, collision free configurations for tensegrity based robots," in *Intelligent Robots and Systems, 2008. IROS 2008. IEEE/RSJ International Conference on*, 3769-3774.

Yu, C.-H. Haller, K. Ingber, D. and Nagpal, R. (2008) "Morpho: A self-deformable modular robot inspired by cellular structure," in *Intelligent Robots and Systems, 2008. IROS 2008. IEEE/RSJ International Conference on*, 3571-3578.

Busscher, I. Ploegmakers, J. J. Verkerke, G. J. and Veldhuizen, A. G. (2010) "Comparative anatomical dimensions of the complete human and porcine spine," *European spine journal,* vol. 19, 1104-1114.

Been, E. and Kalichman, L. (2014) "Lumbar lordosis," *The Spine Journal,* vol. 14, 87-97.

Mejia, E. A. Hennrikus, W. L. Schwend, R. M. and Emans, J. B. (1996) "A prospective evaluation of idiopathic left thoracic scoliosis with magnetic resonance imaging," *Journal of Pediatric Orthopaedics,* vol. 16, 354-358.

Sonsa, (2016) " Anatomy of the Spine," ed.

Masharawi, Y. Salame, K. Mirovsky, Y. Peleg, S. Dar, G. Steinberg, N. and Hershkovitz, I. (2008) "Vertebral body shape variation in the thoracic and lumbar spine: characterization of its asymmetry and wedging," *Clinical Anatomy,* vol. 21, 46-54.

Bernhardt, M. (1997)"Normal sagittal plane alignment," *The textbook of spinal surgery*.

Knox, J. B. and Lonner, B. S. (2014) "Sagittal Balance," in *Minimally Invasive Spinal Deformity Surgery*, ed: Springer, 33-37.

Roussouly, P. and Pinheiro-Franco, J. L. (2011) "Sagittal parameters of the spine: biomechanical approach," *European spine journal,* vol. 20, 578.

Vrtovec, T. Pernuš, F. and Likar, B. (2009) "A review of methods for quantitative evaluation of spinal curvature," *European spine journal,* vol. 18, 593-607.

Oh, C. L. Choong, K. K. Nishimura, T. and Kim, J. Y. (2016) "Form-finding of human spine inspired biotensegrity," in *Proceedings of the IASS Annual Symposium 2016 "Spatial Structures in the 21st Century"*, Tokyo, Japan.